

## PHOTOMETRIC REVERBERATION MAPPING OF ACTIVE GALACTIC NUCLEI

Michael Ramolla,<sup>1</sup> Francisco Pozo Nuñez,<sup>1</sup> Christian Westhues,<sup>1</sup> Martin Haas,<sup>1</sup> Rolf Chini,<sup>1,2</sup> Katrien Steenbrugge,<sup>2</sup> Roland Lemke,<sup>1</sup> and Miguel Murphy<sup>2</sup>

### RESUMEN

Photometric reverberation mapping es un método novedoso utilizado para determinar el tamaño y geometría de la región de línea ancha (BLR) en núcleos de galaxias activas (AGN) al igual que el brillo de sus galaxias. Establecer una relación estrecha de luminosidad - tamaño BLR puede permitir que los AGN de tipo 1 sean usados como marcadores de distancia cosmológica. Sin embargo, la calidad de los resultados es más sensible a un muestreo temporalmente denso y continuidad de las curvas fotométricas. Esto exige un observatorio, con condiciones ambientales óptimas, como el "Universitätssternwarte Bochum", ubicado en el desierto de Atacama en Chile. La gran cantidad de observaciones son controlados robóticamente, adaptando el plan de observación a las condiciones climáticas. Acá presentamos los primeros resultados prometedores de nuestros estudios.

### ABSTRACT

Photometric reverberation mapping is a novel method used to determine the size and geometry of the broad line region (BLR) in active galactic nuclei (AGN) as well as their host galaxy free luminosities. Establishing a tight luminosity - BLR-size relation may allow type-1 AGN to be used as cosmological distance probes. However, the quality of the results is most sensible to dense time sampling and continuity of the photometric lightcurves. This demands an observatory, with optimal environmental conditions, like the "Universitätssternwarte Bochum", located in the Atacama Desert in Chile. The massive amount of observations are controlled robotically, adapting observational schedules of the telescopes to the weather conditions. Here we present one of the first promising results of our studies.

*Key Words:* galaxies: active — galaxies: nuclei — galaxies: distances and redshifts — galaxies: seyfert — quasars: emission lines

### 1. INTRODUCTION

Reverberation mapping (RM) (Blandford & McKee 1982), where the reaction of the broad line region (BLR) to variations of the continuum emitting central region is measured, has been performed for only about 70 AGN in the last three decades. Usually, this is based on spectroscopic observations that quickly require very large telescopes. There appears to be a relation between the nuclear luminosity and BLR size  $R \propto L^\alpha$  (Koratkar & Gaskell 1991), which is expected theoretically to have  $\alpha = 0.5$  (Netzer 1990). In order to efficiently increase the sample of measured BLR sizes together with the AGNs nuclear luminosity, a photometric approach is desirable. Recently, the "Universitätssternwarte Bochum"<sup>3</sup> (USWB), which is about 20km close to the Paranal Observatory, performed the first successful photometric narrow band RM observations

of AGN that led to successful measurements of  $H\alpha$  and  $H\beta$  sizes (Haas et al. 2011; Pozo Nuñez et al. 2012, 2013; Ramolla 2012; Ramolla et al. 2013) and also of the dust torus size (Pozo Nuñez et al. 2014). Here we demonstrate our approach on the Seyfert 1 galaxy ESO 399-IG20 (Pozo Nuñez et al. 2013), which also allows modeling of the BLR geometry, giving us the possibility to rule out a spherical shell geometry of the BLR, compared to a more suitable low ( $6^\circ$ ) inclination disk-like structure.

### 2. DATA

Our photometric long-term studies are accompanied by follow-up spectroscopy. In most cases, we are supplied with single epoch spectra from the Calar Alto Faint Object Spectrograph (CAFOS) in Spain, but also from the South African Large Telescope (SALT).

In case of ESO399-IG20 (Pozo Nuñez et al. 2013), observations have been performed with the 15cm Robotic Bochum Twin Telescope (RoboTT) from May 2011 until Nov 2011. We use one of the twin telescopes to record a sequence of  $[SII]\lambda 6721 \pm 30$

<sup>1</sup>Astronomisches Institut, Ruhr-Universität Bochum, Universitätsstraße 150(ramolla@astro.rub.de).

<sup>2</sup>Facultad de Ciencias, Universidad Católica del Norte, Antofagasta, Chile.

<sup>3</sup>[http://www.astro.rub.de/Astrophysik/all\\_infos.html](http://www.astro.rub.de/Astrophysik/all_infos.html)

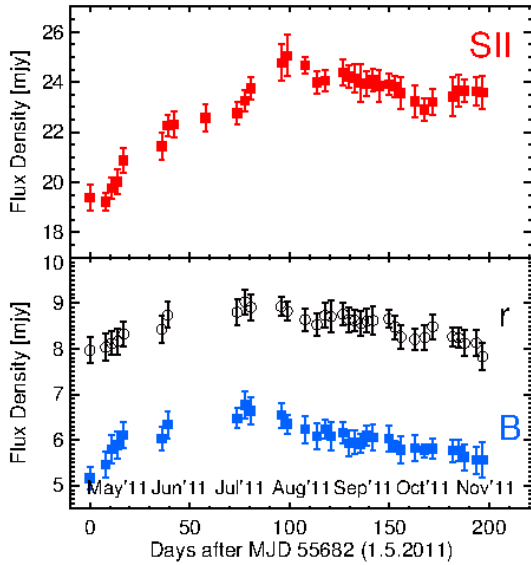


Fig. 1. The extinction corrected lightcurves for the 7<sup>5</sup> aperture photometry of ESO 399-IG20.

images, while the other is used simultaneously with available broad Johnson *B* or Sloan *r* filters.

Data reduction was performed using IRAF, SExtractor (Bertin & Arnouts 1996), SCAMP (Bertin 2006) and SWarp (Bertin 2010) in the same manner as described by Haas et al. (2012), using an 7<sup>5</sup> diameter aperture for flux extraction.

The lightcurve of the AGN is obtained by measuring its flux relative to the 30 closest non-variable stars on the same image. The absolute calibration is performed afterwards, using fields of Landolt (2009) that are observed on the same night as the AGN and considering the atmospheric extinction of (20km nearby) Paranal Patat et al. 2011 and the galactic foreground extinction as determined by Patat et al. (2011).

### 3. RESULTS AND DISCUSSION

Figure 1 shows the resulting lightcurves of ESO 399-IG20. In both, *r* and *B* band, there is a clear rise of the lightcurve, peaking at end of July. In the narrow [SII] band, this peak appears to be shifted to early August.

To remove the continuum flux inside our [SII] NB filter, we must subtract a suitable fraction of the red *r* band continuum lightcurve (dominated by continuum flux) from the NB. By plotting the NB flux against the underlying Sloan *r* band flux, the average fraction of continuum in the NB filter is  $\sim 30\%$  for ESO 399-IG20.

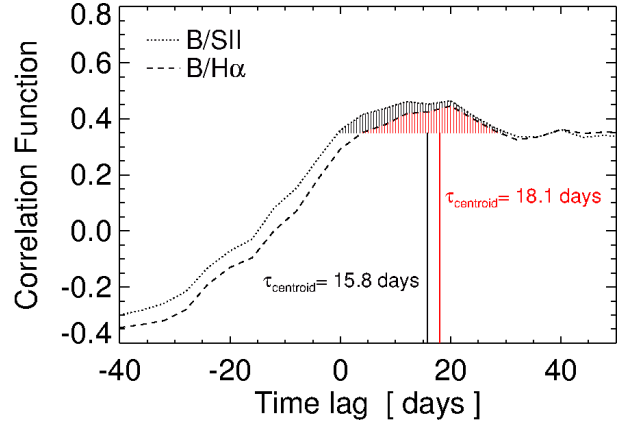


Fig. 2. DCF for the ESO 399-IG20 photometric lightcurves from the 2011 epoch. The dashed line represents the correlation between *B* and  $H\alpha$  and the dotted line the correlation between *B* band and uncorrected [SII] filter flux. Filled areas represent 90% of the peak correlation. Red for *B*- $H\alpha$  and black for *B*-[SII]. The vertical lines represent the centroid of the filled areas.

To determine the time delay between the *B* band variation and the  $H\alpha$  response we determine the discrete correlation function (DCF) by Edelson & Krolik (1988). Figure 2 shows the DCF for *B*- $H\alpha$  with a centroid delay  $\tau_{\text{cen}}$  of 18.1days while the *B*-[SII] has 15.8days. The latter result is not unexpected, because the [SII] band still contains the red continuum which is almost auto-correlated ( $\tau = 0$ ) to a *B* band variation.

A statistical analysis of this result is performed using the flux randomization / random subset selection (FR/RSS) method by Peterson et al. (1998). In this method, 2000 different lightcurves are generated from the original flux data and varied within standard deviation of the measurements. Then, from each lightcurve a random subset is subtracted until 63% of the original data points is left. For all 2000 generated lightcurves, we determine the DCF peak centroid as performed above. From the distribution of obtained  $\tau_{\text{cen}}$  values we obtain  $\tau = 18.7^{+2.5}_{-2.2}$  for the delay between *B* band continuum and  $H\alpha$ . Correcting for the time dilation of a redshift of  $z = 0.025$ , we obtain a rest frame lag of  $18.2^{+2.4}_{-2.1}$  days. In the detailed analysis of the cross correlation between the broad bands *B* and *r* in Pozo Nuñez et al. (2013), using the method proposed by Chelouche & Daniel (2012), we can retrieve a *B*- $H\alpha$  lag of  $17.5 \pm 3.1$  days that is in agreement with the result above.

As performed in Haas et al. (2011) and Pozo Nuñez et al. (2012), we apply the flux variation gradient method, first introduced by Choloniewski (1981), on our broad *B* and *r* band fluxes. Both

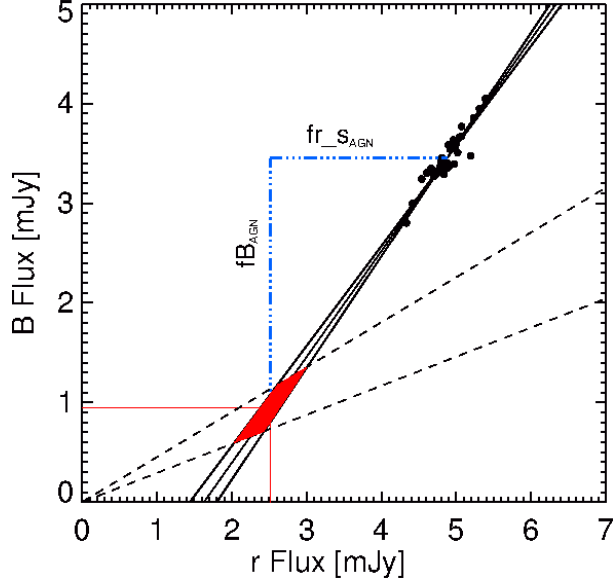


Fig. 3. Flux variation gradient of ESO 399-IG20 for  $B$  and  $r$  band flux. Dashed lines mark the host slope range of Sakata et al. (2010). Our data is approximated by an OLS-bisector fit (three drawn through black lines:  $+1\sigma$ , average,  $-1\sigma$ ). The red filled area marks the intersection of host and AGN color slopes.

fluxes, which were taken consecutively at the same night, are plotted in a flux-flux diagram (our Fig. 3). While the Host stays constant, the AGN flux varies in both filters that are dominated by continuum emission. Notably, the color is staying constant. As a result, the variation of the AGN in this diagram has a linear slope, which we approximate by an ordinary least squares (OLS) bisector fit. From the analysis of low redshift ( $z < 0.03$ ) AGN host galaxy colors by Sakata et al. (2010), we adopt a range of typical host colors  $0.4 < \Gamma_{BV}^{\text{host}} < 0.53$ . Because the AGN has a significantly bluer slope, we are able to disentangle host from AGN flux in the bands at the intersection of the different color slopes of host and AGN. The host-free average AGN fluxes are depicted by the blue dashed lines in the Figure. From these AGN fluxes we can interpolate the monochromatic AGN luminosity  $\lambda L_{\lambda, \text{AGN}}$  at  $5100\text{\AA}$  as detailed in Pozo Nuñez et al. (2012). For a luminosity distance of  $102\text{Mpc}^4$  we obtain  $\lambda L_{\lambda, \text{AGN}} = (1.69 \pm 0.25) \times 10^{43} \text{ergs}^{-1}$ .

We can compare our results with the R-L data of  $H\beta$  by Bentz et al. (2013), using the  $\tau(H\alpha) : \tau(H\beta)$  scaling factor of 1.54, obtained by Bentz et al. (2010), showing that ESO 399-IG20 lies very close to the

<sup>4</sup>adopting a standard cosmological model with  $H_0 = 73 \text{km s}^{-1} \text{Mpc}^{-1}$ ,  $\Omega_M = 0.27$  and  $\Omega_\Lambda = 0.73$

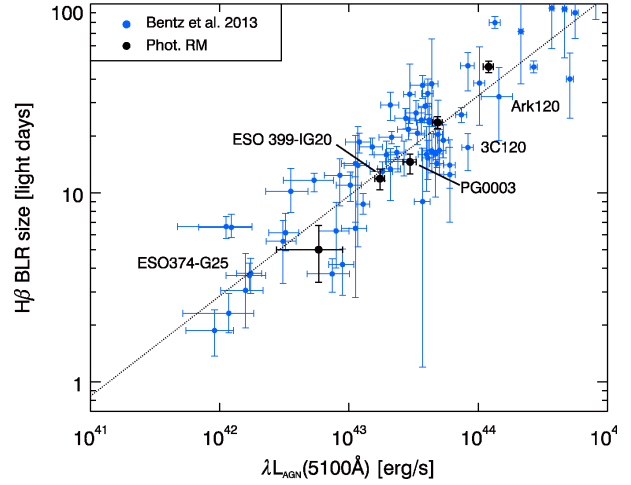


Fig. 4. BLR radius vs monochromatic AGN Luminosity at  $5100\text{\AA}$ . New photometric values by our group are shown in black. The value of ESO 374-G25 is taken from Ramolla (2012).

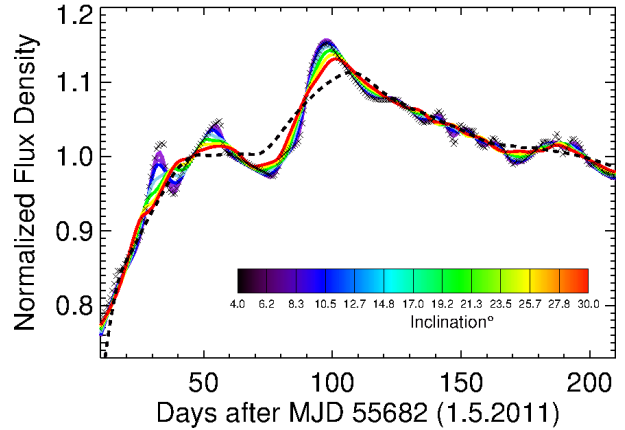


Fig. 5. Interpolated  $H\alpha$  lightcurve (black crosses) with the results of best fit models of a spherical shell BLR (dashed line) and multiple disk-like BLR with inclinations from  $0$  to  $10^\circ$ , represented by colored lines.

best slope of the distribution in Figure 4.

From a well sampled lightcurve, as of ESO 399-IG20, we may extract limitations for possible geometric models of the BLR. Following the models presented by Welsh & Horne (1991) we will analyse the properties of a spherical shell and a thin disk, simulating  $H\alpha$  lightcurves with  $B$  band lightcurves as input signal.

Before we use our measured lightcurves as input for a model, we have to interpolate the gaps in them adequately (compare Fig 1). Instead of a simple linear interpolation, we apply the Stochastic Process Estimation for AGN Reverberation (SPEAR)

method by Zu et al. (2011) that assumes a damped random walk for the variations. Correlating our  $B$  and  $H\alpha$  lightcurve data with the SPEAR algorithm offers a rest-frame time delay of  $17.9 \pm 1.1$  days which is consistent with our FR/RSS method. The interpolated  $H\alpha$  flux curve is shown in Fig. 5. The interpolated  $B$  band flux is used as input for our geometric models. For inner  $r_i$  and outer  $r_o$  boundaries of 16 and 20 light-days, the transfer functions of our models reproduce a variety of  $H\alpha$  lightcurves as seen in Fig. 5. Evidently, the spherical model is unable to trace the rapid variations seen in the  $H\alpha$  lightcurve, while a low inclination disk can reproduce the data very closely. Through  $\chi^2$  minimization for different inclinations  $i$ , we obtain a best fit inclination of  $(6 \pm 3)^\circ$  for ESO 399-IG20.

#### 4. SUMMARY AND OUTLOOK

We presented the results of our photometric reverberation mapping (PRM) campaign for the Seyfert 1 galaxy ESO 399-IG20, employing a combination of broad and narrow bands on a robotic 15cm refractor telescope, located at the USWB in Chile.

1. The  $H\alpha$  BLR has a rest frame size, determined with the FR/RSS method is  $\tau = (18.2^{+2.4}_{-2.1})$  days and consistent with other popular approaches, such as broad band PRM and the SPEAR method.
2. We successfully separated the AGN luminosity from the host contribution, using the FVG method. The resulting monochromatic luminosity of ESO 399-IG20 at  $5100\text{\AA}$  is  $\lambda L_{\lambda, \text{AGN}} = (1.69 \pm 0.25) \times 10^{43} \text{ergs}^{-1}$ . In the R-L diagram, the AGN lies close to the best fit.
3. Using  $B$  band flux as model input, a spherical BLR fails to reproduce the rapid variations observed in our  $H\alpha$  lightcurve. The shape of the BLR variation is best approximated by a thin disk with inclination  $i = (6 \pm 3)^\circ$

All in all, PRM has proven to be a reliable method to determine the BLR size and shape and to extract the host-free AGN luminosity.

With the recent start of operations of an 80cm infra-red and a 40cm optical telescope (Ramolla et al. 2013) at USWB, more measurements can be expected in the near future.

#### REFERENCES

- Bentz, M. C., Denney, K. D., Grier, C. J., et al. 2013, ApJ, 767, 149
- Bentz, M. C., Walsh, J. L., Barth, A. J., et al. 2010, ApJ, 716, 993
- Bertin, E. 2006, Astronomical Data Analysis Software and Systems XV, 351, 112
- . 2010, astrophysics Source Code Library
- Bertin, E. & Arnouts, S. 1996, A&AS, 117, 393
- Blandford, R. D. & McKee, C. F. 1982, ApJ, 255, 419
- Chelouche, D. & Daniel, E. 2012, ApJ, 747, 62
- Cholomiewski, J. 1981, AcA, 31, 293
- Edelson, R. A. & Krolik, J. H. 1988, ApJ, 333, 646
- Haas, M., Chini, R., Ramolla, M., et al. 2011, A&A, 535, A73
- Haas, M., Hackstein, M., Ramolla, M., et al. 2012, AN, 333, 706
- Koratkar, A. P. & Gaskell, C. M. 1991, ApJ, 370, L61
- Landolt, A. U. 2009, AJ, 137, 4186
- Netzer, H. 1990, 20. Saas-Fee Advanced Course of the Swiss Society for Astrophysics and Astronomy: Active galactic nuclei, 57
- Patat, F., Moehler, S., O'Brien, K., et al. 2011, A&A, 527, A91
- Peterson, B. M., Wanders, I., Horne, K., et al. 1998, PASP, 110, 660
- Pozo Nuñez, F., Haas, M., Chini, R., et al. 2014, A&A, 561, L8
- Pozo Nuñez, F., Ramolla, M., Westhues, C., et al. 2012, A&A, 545, A84
- Pozo Nuñez, F., Westhues, C., Ramolla, M., et al. 2013, A&A, 552, A1
- Ramolla, M. 2012, Bochum, Univ., Diss., 2012, UB25647, 101
- Ramolla, M., Drass, H., Lemke, R., et al. 2013, AN, 334, 1115
- Sakata, Y., Minezaki, T., Yoshii, Y., et al. 2010, ApJ, 711, 461
- Welsh, W. F. & Horne, K. 1991, ApJ, 379, 586
- Zu, Y., Kochanek, C. S., & Peterson, B. M. 2011, ApJ, 735, 80